Robust Monotonically Convergent Spatial Iterative Learning Control: Interval Systems Analysis via Discrete Fourier Transform

Berk Altın, *Member, IEEE*, Zhi Wang, *Student Member, IEEE*, David J. Hoelzle, *Member, IEEE*, and Kira Barton, *Member, IEEE*

Additive manufacturing (AM) systems use a layer-by-layer paradigm to build three-dimensional structures. There are myriad of advantages to AM; however, challenges with real-time actuation and sensing relegate AM processes to be largely open-loop processes. In this paper, we build upon the spatial iterative learning control (SILC) strategy to close the loop in the iteration domain in AM systems, enabling autonomous process control in the absence of real-time sensing. We approximate the steady-state partial differential equations of AM systems by discrete two-dimensional convolution operators, and assume uncertain spatially-varying kernels to have a more realistic representation of these complex processes. From this system description, we formalize the robust monotonic convergence (RMC) criterion for SILC. Importantly, we use discrete Fourier transform-based tools to study spatial dynamics, a practical framework for data-rich spatial sensors used in AM. The theoretical results are complemented with experiments on the AM process electrohydrodynamic jet printing, demonstrating that the RMC criterion can predict the design boundary for convergent behavior for norm-optimal SILC.

***Index Terms*—Iterative learning control, discrete Fourier transforms, layered manufacturing, process control, robustness.**

I. Introduction

ADDITIVE manufacturing (AM) technologies have attracted significant attention in recent years, in particular due to advanced capabilities not available with traditional manufacturing methodologies. As opposed to traditional subtractive manufacturing methods such as milling, AM employs a layer-by-layer sequence of selective additions of two-dimensional (2D) layers of materials to build up three-dimensional (3D) parts [1]. AM is advantageous for applications in which complex parts are needed in low volumes; examples include fuel nozzles for aircraft engines [2], custom implants [3], and custom fixtures and dies for injection molding [4]. Despite these advantages, almost all AM systems operate in an open-loop manner [1], wherein processes are tuned by human operators by trial-and-error, which limits manufactured part quality as processes are susceptible to variability in material feedstocks and environmental conditions.

The limitations of AM systems discussed above point towards feedback control as a potential solution to improve the performance of these complex, uncertain processes. However, it is very challenging to sense and actuate AM systems in real time. In particular, 1) material addition is distributed and requires distributed sensing such as computationally-intensive optical and thermal machine-vision feedback [5], 2) sensors are often noncollocated (in space or time) with the output, as it is difficult, and sometimes impossible, to place a sensor at the location of material addition, and 3) existing sensing techniques often have inadequate resolutions at submicron length scales, or insufficient sampling rates that can fail to convey meaningful information on fast processes, where it might be necessary to detect high-frequency changes. Taken together, conventional feedback controllers often cannot be applied to the process regulation problem.

The unique challenges of AM control, along with the layer-by-layer nature of AM, make recursive control a powerful substitute for feedback control: in the absence of real-time feedback, data-rich optical/thermal images or topographical measurements can be processed in between each layer to update the process input and improve part quality in a run-to-run fashion. This mode of offline operation (operate system, measure output, update input) is often called run-to-run control [6] and can be applied to systems that use post-process sensors when it is infeasible or impractical to measure the output in real time; example sensing modes include laser profilometry of a machined surface [7], computationally-intensive machine-vision processed data [3], [8], and wireless systems in which the reference trajectory sampling rate exceeds the sensor signal transmission rate [9]. The offline run-to-run control methodology can also be recognized as the iterative learning control (ILC) paradigm, wherein the objective is to iteratively construct the feedforward input that would achieve a desired reference (or its approximation) using input-output data from prior iterations [10], [11]. It is important to note that ILC has been traditionally applied to decrease the magnitude of the *temporal* tracking error $e(t)$ of systems defined by ordinary differential/difference equations. In contrast, AM quality is defined by dimensional fidelity, thus the control objective is to reduce the magnitude of a spatial error function $e(x, y)$, where x and y are spatial coordinate arguments in a 2D Cartesian coordinate system.

This paper builds on the lifted- and frequency-domain representations of spatial iterative learning control (SILC)

Manuscript received January 0, 2017. This work was supported by the NSF grants CMMI-1334204, CMMI-1434693, and CMMI-1727894, and conducted while the first and third authors were with the Department of Electrical Engineering and Computer Science at the University of Michigan, and the Department of Aerospace and Mechanical Engineering at the University of Notre Dame, respectively.

B. Altin is with the Department of Computer Engineering, University of California, Santa Cruz, CA USA (e-mail: berkaltin@ucsc.edu).

Z. Wang is with the Department of Aerospace and Mechanical Engineering, University of Notre Dame, Notre Dame, IN 46556 USA (e-mail: zwang10@nd.edu).

D. J. Hoelzle is with the Department of Mechanical and Aerospace Engineering, the Ohio State University, Columbus, OH 43210 USA (e-mail: hoelzle.1@osu.edu).

K. Barton is with the Department of Mechanical Engineering, University of Michigan, Ann Arbor, MI, 48109 USA (e-mail: bartonkl@umich.edu).

introduced in [12] by discussing certain aspects of the SILC problem pertaining specifically to AM, and developing frequency-domain methods that ensure robust monotonic convergence (RMC) in this setting. The principal contribution is the extension of the problem to uncertain and spatially-varying convolution operators, enabling a more realistic modeling framework for these complex processes. To maintain the computational-efficiency associated with the discrete Fourier transform (DFT) so that large datasets from a spatial sensor are usable [12], the 2D convolution operators are assumed to be subject to spatially-invariant bounds, equivalently modeled as interval uncertainties with circulant symmetry on the lifted plant matrix.

The tools developed here to address the problem are strongly motivated by the target application area of AM. However, it should be noted that they can be used in other application areas such as distributed irrigation [13] and material removal processes (e.g. long-wall coal mining, turning lathe operations, excavation), and find use in 1D temporal/spatial systems, as evidenced by the work presented in [14] that relies on the one-dimensional (1D) DFT for synthesis and analysis. It is also important to mention that we utilize SILC to improve part quality of a product built in a single layer, from one substrate to the next. For this reason, the multidimensional repetitive process framework [15], which can model the layer-by-layer dynamics that arise from printing multi-layer parts in AM applications, is not considered here.

The rest of the paper is organized as follows: Section II introduces our style of notation and presents certain preliminaries. Section III defines the interval uncertainty model in the lifted matrix representation and discusses SILC convergence properties of interval systems. In Section IV, we estimate the maximum allowable interval uncertainty for a given nominal update law and plant using interval stability radii. Section V briefly discusses the applicability of the results to iteration-varying models and disturbances. Section VI suggests using the stability radius in an optimization problem to synthesize the ILC update law. Section VII demonstrates the usefulness of the stability radius based RMC criterion via experimental results on a microscale electrohydrodynamic jet printing system. Concluding remarks are given in Section VIII. For a more streamlined presentation, complementary material and proofs of certain results are given in Appendices A, B, and C.

II. Preliminaries: DFT-Based Iterative Learning Control

In this section we discuss the background necessary for the analysis of the SILC strategy in the lifted and frequency domains. In addition, we introduce the style of notation to be used throughout the paper.

A. Notation

We use $\mathbb{Z}$ to represent the set of integers and $\mathbb{N}$ its nonnegative subset. For an odd positive integer n, we define the n element set

$$\mathbb{Z}_n \triangleq \{(1-n)/2, (3-n)/2, \ldots, (n-1)/2\}$$

if $n > 1$, and $\mathbb{Z}_n = \mathbb{Z}_1 \triangleq \{0\}$ if $n = 1$. For example, for the case of $n = 5$, we have $\mathbb{Z}_n = \mathbb{Z}_5 \triangleq \{-2, -1, 0, 1, 2\}$. In the same manner, given any generic scalar function $p(x, y)$, where $(x, y) \in \mathbb{Z}_m \times \mathbb{Z}_n$, its equivalent $m \times n$ matrix representation is given as

$$\begin{bmatrix} p\left(\frac{1-m}{2}, \frac{1-n}{2}\right) & p\left(\frac{1-m}{2}, \frac{3-n}{2}\right) & \cdots & p\left(\frac{1-m}{2}, \frac{n-1}{2}\right) \\ p\left(\frac{3-m}{2}, \frac{1-n}{2}\right) & p\left(\frac{3-m}{2}, \frac{3-n}{2}\right) & \cdots & p\left(\frac{3-m}{2}, \frac{n-1}{2}\right) \\ \vdots & \vdots & \ddots & \vdots \\ p\left(\frac{m-1}{2}, \frac{1-n}{2}\right) & p\left(\frac{m-1}{2}, \frac{3-n}{2}\right) & \cdots & p\left(\frac{m-1}{2}, \frac{n-1}{2}\right) \end{bmatrix}$$

if $m, n > 1$. When either $m = 1$ or $n = 1$, $p(x, y)$ can be expressed as an $m \times n$ matrix in a similar fashion. For instance, for $p(x, y) = x + y$, $m = 3$ and $n = 5$, we have the equivalent matrix representation

$$\begin{bmatrix} -3 & -2 & -1 & 0 & 1 \\ -2 & -1 & 0 & 1 & 2 \\ -1 & 0 & 1 & 2 & 3 \end{bmatrix},$$

and for $p(x, y) = x + y^2 + 2$, $m = 1$ and $n = 3$, we have the equivalent matrix representation $\begin{bmatrix} 3 & 2 & 3 \end{bmatrix}$. We will use $p(x, y)$ interchangeably to refer to the function or its equivalent matrix representation. The 2D DFT of $p(x, y)$ will be denoted $P(u, v)$, where $(u, v) \in \mathbb{Z}_m \times \mathbb{Z}_n$ is the spatial frequency; $P(u, v)$ will also have an equivalent matrix representation in the same manner and will be used interchangeably as a function or a matrix. Let p be a matrix. Then, p^T (p^*) is the transpose (Hermitian transpose) of p, and $[p]_{ij}$ denotes the element in the i-th row and j-th column of p. We define the operator $\mathcal{V}$ so $\mathcal{V}(p) \triangleq \mathrm{vec}(p^T)$, where $\mathrm{vec}(.)$ is the conventional (columnwise) vectorization operator. The Hadamard (entrywise) product of two matrices is denoted by $\circ$. Let $p_1, p_2, \ldots, p_n$ be square matrices. Then $\mathrm{diag}(p_1, p_2, \ldots, p_n)$ is a block diagonal matrix where the ith element of the the block diagonal is p_i. Similarly, $\mathrm{circ}(p_1, p_2, \ldots, p_n)$ denotes a block circulant matrix in which the ith block of the middle column partition is p_i, where n is odd; e.g.

$$\mathrm{circ}(p_1, p_2, p_3) = \begin{bmatrix} p_2 & p_1 & p_3 \\ p_3 & p_2 & p_1 \\ p_1 & p_3 & p_2 \end{bmatrix}.$$

The notation $\mathrm{Circ}(m, n)$ represents the set of all real block circulant matrices with circulant blocks (BCCB), where the block partition size is $m \times m$ and the size of each block is $n \times n$. The symbols $\preccurlyeq$ and $\succcurlyeq$ will be used to denote elementwise inequalities; e.g $p_1 \preccurlyeq p_2$ means that $[p_1]_{ij} \leq [p_2]_{ij}$ for each i, j. The modulus of a complex number is denoted $|.|$. On a final note, $\|.\|_{\mathfrak{p}}$ denotes the induced $\mathfrak{p}$-norm for matrices and the vector $\mathfrak{p}$-norm for vectors, where $\mathfrak{p} \in [1, \infty]$.

B. Motivation for the DFT-based Approach

To get an insight into the need for DFT-based algorithms, we revisit the ILC problem of discrete linear systems in the temporal domain. It is well known that every linear operator on a finite-dimensional vector space has a matrix representation. In linear discrete-time ILC, this property is used to convert

the 2D control problem into the feedback control problem of a static multi-input multi-output system. For example, consider a single-input single-output linear discrete-time system with impulse response $h(k)$, input $f_j(k)$, and output $g_j(k)$, for every $k \in \{0, 1, \ldots, n\}$ and $j \in \mathbb{N}$, where, without loss of generality, we assume $h(0) = 0$ and $h(1) \neq 0$. Then, we can cast the convolution sum into the matrix form

$$\underbrace{\begin{bmatrix} g_j(1) \\ g_j(2) \\ \vdots \\ g_j(n) \end{bmatrix}}_{\mathbf{g}_j} = \underbrace{\begin{bmatrix} h(1) & 0 & \ldots & 0 \\ h(2) & h(1) & \ldots & 0 \\ \vdots & \vdots & \ddots & \vdots \\ h(n) & h(n-1) & \ldots & h(1) \end{bmatrix}}_{\mathbf{H}} \underbrace{\begin{bmatrix} f_j(0) \\ f_j(1) \\ \vdots \\ f_j(n-1) \end{bmatrix}}_{\mathbf{f}_j}$$

for all $j \in \mathbb{N}$. This procedure is commonly called *lifting*, and the system above is said to be in lifted form with the supervectors $\mathbf{g}_j$ and $\mathbf{f}_j$, which enables the control engineer to employ matrix methods in the design and analysis of the ILC problem.[1] However, it is also easy to see that this methodology is not suitable for large n: The most general first-order update law $\mathbf{f}_{j+1} = \mathbf{L_f} \mathbf{f}_j + \mathbf{L_e} \mathbf{e}_j$, where the error vector is defined as $\mathbf{e}_j \triangleq \mathbf{g}_d - \mathbf{g}_j$ for a given reference vector $\mathbf{g}_d$, involves two matrix-vector multiplications, which are $\mathcal{O}(n^2)$ operations. For AM systems, the curse of dimensionality is amplified because the spatial sensors employed (machine vision, profilometry, etc.) are data intensive. To mitigate this issue, the 2D spatial analog of this update law will be implemented using the DFT, via Fast Fourier Transform (FFT) algorithms [12]. This reduces computational complexity of the update law to $\mathcal{O}(n \log n)$ since FFT algorithms are $\mathcal{O}(n \log n)$, and the matrix-vector product simplifies to the Hadamard (entrywise) product of two vectors in the discrete frequency domain. We refer the readers to [16]–[18] for discussions of computational efficiency in ILC.

Remark 1. *While it is possible to rely on a multidimensional systems framework to overcome computational limitations, the variety of algorithms that can be tractably synthesized and analyzed in this setting is relatively limited. The lifted-domain representation offers the ability to process large amounts of data via a variety of algorithms through matrix methods, and DFT-based algorithms form an important subset of these methods characterized by computational efficiency. The usefulness of the DFT-based approach to ILC has been demonstrated previously in the 1D temporal case in [14].*

C. Equivalent Representations of the Plant

Consider a single-input single-output linear partial differential equation (PDE) with independent spatial variables x, y on a compact domain, and the temporal variable t. It is assumed that the PDE is causal, time- and spatially-invariant, and given a bounded input with compact support that is *constant in-time*, the PDE generates a bounded output that converges to a steady-state distribution in an appropriate function norm [12]. Since the steady-state input-output behavior of this PDE can be represented by aid of the Green's function, we will develop a discretized convolution representation for the spatial plant H that models the behavior of the steady-state PDE.

Let X be the space of all functions $p : \mathbb{Z}^2 \to \mathbb{R}$. Then, a spatially-invariant linear operator $H : X \to X$ can be represented by the convolution sum

$$g_j(x, y) = \sum_{\substack{m \in \mathbb{Z} \\ n \in \mathbb{Z}}} h(x - m, y - n) f_j(m, n)$$

for all $j \in \mathbb{N}$ and $(x, y) \in \mathbb{Z}^2$, where $h(x, y)$ is the spatial impulse response associated with H. Note that contrary to its 1D temporal counterpart, the above equation is "non-causal" in space. We will assume that $h(x, y)$ and $f_j(x, y)$ have finite support; in the case that $h(x, y)$ extends towards infinity, we will assume that it has negligible magnitude outside of a finite grid. More specifically, we assume that $h(x, y) = 0$ for every $(x, y) \notin \mathbb{Z}_A \times \mathbb{Z}_B$, and $f_j(x, y) = 0$ for every $(x, y) \notin \mathbb{Z}_C \times \mathbb{Z}_D$ and $j \in \mathbb{N}$. As is typical in the image processing literature, the above can then be rewritten as

$$g_{+,j}(x, y) = \sum_{\substack{m \in \mathbb{Z}_M \\ n \in \mathbb{Z}_N}} h_+(x - m, y - n) f_{+,j}(x, y) \qquad (1)$$

for all $j \in \mathbb{N}$ and $(x, y) \in \mathbb{Z}_M \times \mathbb{Z}_N$, where the subscript $+$ denotes the zero-padded extensions of the functions to the domain $\mathbb{Z}_M \times \mathbb{Z}_N$, where $M = A + C - 1$ and $N = B + D - 1$:[2]

$$f_{+,j}(x, y) \triangleq \begin{cases} f_j(x, y), & \text{if } (x, y) \in \mathbb{Z}_A \times \mathbb{Z}_B \\ 0, & \text{otherwise} \end{cases},$$

$$h_+(x, y) \triangleq \begin{cases} h(x, y), & \text{if } (x, y) \in \mathbb{Z}_C \times \mathbb{Z}_D \\ 0, & \text{otherwise} \end{cases},$$

From hereinafter, the subscript $+$ will be dropped and we will assume that all relevant functions are properly extended. The zero-padding process introduces coordinates in the input vector that are constrained to be zero, which means that we have complete freedom in choosing the elements of the matrix $\mathbf{H}$ in the columns that correspond to said coordinates. In a way, we introduce a pseudo-periodicity in the impulse response so that we can utilize the DFT to our advantage. As a result of the zero-padding procedure, we can recover a plant matrix $\mathbf{H}$ that is BCCB, which enables us to use the 2D DFT during control synthesis and analysis:

$$\mathbf{g}_j = \mathbf{H} \mathbf{f}_j \quad \forall j \in \mathbb{N}, \qquad (2)$$

where $\mathbf{H} \triangleq \operatorname{circ}(\mathbf{H}_{(1-M)/2}, \mathbf{H}_{(3-M)/2}, \ldots, \mathbf{H}_{(M-1)/2})$,

$$\mathbf{H}_i \triangleq \operatorname{circ}(h(i, (1-N)/2), h(i, (3-N)/2), \ldots, h(i, (N-1)/2)) \quad \forall i \in \mathbb{Z}_M,$$

and $\mathbf{g}_j \triangleq \mathcal{V}(g_j(x, y))$, $\mathbf{f}_j \triangleq \mathcal{V}(f_j(x, y))$. The plant operator $\mathbf{H}$ has the eigendecomposition $\mathbf{W}^* \mathbf{\Lambda_H} \mathbf{W}$, where $\mathbf{W}$ is a unitary matrix that is invariant over $\operatorname{Circ}(M, N)$, and

[1] We will use this bold-faced notation to represent signals and systems in lifted form.

[2] The assumption that A, B, C, D are odd integers is rather for convenience, so that functions and their extensions have defined center coordinates.

the eigenvalue matrix $\mathbf{\Lambda_H} \triangleq \mathrm{diag}(\mathcal{V}(H(u,v)))$. The complex matrix $\mathbf{W}$ is also the matrix representation of the *normalized* 2D DFT; e.g. for the 2D function $f_j(x,y)$, its Fourier transform is $\mathcal{V}(F_j(u,v)) = \sqrt{MN}\mathbf{W}\mathbf{f}_j$. Conversely, for any $\mathbf{H} \in \mathrm{Circ}(M,N)$, one can extract a 2D impulse response function by taking the inverse DFT of its eigenvalue matrix $\mathbf{\Lambda_H}$, given by the decomposition of $\mathbf{W}^*\mathbf{\Lambda_H}\mathbf{W}$. As a result, we have the following equivalent frequency-domain representation:

$$G_j(u,v) = H(u,v) \circ F_j(u,v) \quad \forall j \in \mathbb{N}. \tag{3}$$

Other relevant properties of the matrix $\mathbf{H}$, and hence BCCB matrices, are listed below without proof. These follow by definition and from the eigendecomposition introduced above; see [12] for further details.

1) The spectral radius and the maximal singular value of $\mathbf{H}$ are equal.
2) $\mathcal{H}_\infty$ *norm*: The induced 2-norm of $\mathbf{H}$ is given by the maximum modulus of its DFT representation; i.e. $\|\mathbf{H}\|_2 = \big\|H(u,v)\big\|_\infty \triangleq \max_{(u,v)\in\mathbb{Z}_M\times\mathbb{Z}_N} |H(u,v)|$.
3) The induced 1-, 2-, and infinity norms of $\mathbf{H}$ satisfy $\|\mathbf{H}\|_2 \leq \|\mathbf{H}\|_1 = \|\mathbf{H}\|_\infty$.

The last property follows from Corollary 2.3.2 of [19], which states the induced norm inequality $\|.\|_2^2 \leq \|.\|_1\|.\|_\infty$.

The representation (3) shows that the computation of the output in the frequency domain requires pointwise multiplication, an $\mathcal{O}(MN)$ operation, as opposed to the lifted form in which we have the $\mathcal{O}((MN)^2)$ matrix multiplication. Thus, for $\mathbf{L_f}, \mathbf{L_e} \in \mathrm{Circ}(M,N)$, it is much faster to take forward transforms, compute

$$F_{j+1}(u,v) = L_f(u,v) \circ F_j(u,v) + L_e(u,v) \circ E_j(u,v),$$

and take the inverse transform to recover $f_{j+1}(x,y)$, via FFT algorithms. Thus, our aim is to synthesize BCCB matrices $\mathbf{L_f}$ and $\mathbf{L_e}$, that are suitable for large-scale computations.

III. Interval Models for Uncertain Systems

AM processes are innately spatially varying as the process physics, described by PDEs on a finite domain, yield input/output responses that can vary significantly from the infinite-domain response near the boundaries. Thus, the spatially-invariant nominal model given in (1), based on the notion of Green's function as the convolution kernel to solve PDEs on the infinite domain, is unrealistic for AM applications. At first glance, this observation suggests a reformulation of (1) to accommodate a spatially-varying convolution kernel. However, a transformation of a spatially-varying form of (1) into the frequency domain does not exist, to the best of the authors' knowledge. To maintain the computational efficiency of the frequency-domain representation, and capture the kernel spatial variation and modeling uncertainties seen in AM, we formulate the problem as that of robustness under *interval uncertainties* with spatially-invariant bounds. Our definitions of interval uncertainties extend the temporal interval uncertainty work of [20], [21] to the SILC framework.

A. Interval Uncertain Plants

The 2D convolution representation of the input-output operator can be easily generalized to accommodate uncertainties and spatial variations in the dynamics of the system:

$$g_j(x,y) \quad = \quad \sum_{\substack{m\in\mathbb{Z}_M \\ n\in\mathbb{Z}_N}} h_{(x,y)}(x - m, y - n) f_j(m,n)$$

for all $j \in \mathbb{N}$ and $(x,y) \in \mathbb{Z}_M \times \mathbb{Z}_N$, where

$$h_{(x,y)}(m,n) \in [\underline{h}(m,n), \bar{h}(m,n)] \qquad \forall (m,n),(x,y) \in \mathbb{Z}_M \times \mathbb{Z}_B.$$

The function $h_{(x,y)}(m,n)$ is the uncertain response to an impulse applied at coordinate (x,y), subject to the lower bound $\underline{h}(m,n)$ and upper bound $\bar{h}(m,n)$. These bounds are chosen to be spatially-invariant based on a hypothetical identification scenario where the system response is measured at a few randomly selected coordinates. The convolution kernel bounds reflect the bounds on spatial variance of the impulse response. In addition, the choice of spatially-invariant bounds are meant to facilitate the usage of DFT-based tools. For analysis purposes, the system can be lifted into the input-output form $\mathbf{g}_j = \mathbf{H}\mathbf{f}_j$, where $\mathbf{g}_j$ and $\mathbf{f}_j$ are the same as before. Although the plant matrix $\mathbf{H}$ is not necessarily BCCB, it is subject to the BCCB bounds $\underline{\mathbf{H}} \preccurlyeq \mathbf{H} \preccurlyeq \bar{\mathbf{H}}$, where

$$\underline{\mathbf{H}} \triangleq \mathrm{circ}(\underline{\mathbf{H}}_{(1-M)/2}, \underline{\mathbf{H}}_{(3-M)/2}, \ldots, \underline{\mathbf{H}}_{(M-1)/2}),$$
$$\bar{\mathbf{H}} \triangleq \mathrm{circ}(\bar{\mathbf{H}}_{(1-M)/2}, \bar{\mathbf{H}}_{(3-M)/2}, \ldots, \bar{\mathbf{H}}_{(M-1)/2}),$$

and

$$\underline{\mathbf{H}}_i \triangleq \mathrm{circ}(\underline{h}(i,(1-N)/2), \underline{h}(i,(3-N)/2), \ldots, \underline{h}(i,(N-1)/2)) \quad \forall i \in \mathbb{Z}_M,$$
$$\bar{\mathbf{H}}_i \triangleq \mathrm{circ}(\bar{h}(i,(1-N)/2), \bar{h}(i,(3-N)/2), \ldots, \bar{h}(i,(N-1)/2)) \quad \forall i \in \mathbb{Z}_M.$$

We also define the set of interval matrices $\mathbf{H}^I$ and the set of vertex matrices $\mathbf{H}^V$:

$$\mathbf{H}^I \triangleq \{\mathbf{P} \in \mathbb{R}^{MN\times MN} : \underline{\mathbf{H}} \preccurlyeq \mathbf{P} \preccurlyeq \bar{\mathbf{H}}\},$$
$$\mathbf{H}^V \triangleq \{\mathbf{P} \in \mathbf{H}^I : [\mathbf{P}]_{ij} \in \{[\underline{\mathbf{H}}]_{ij}, [\bar{\mathbf{H}}]_{ij}\}, (i,j) \in (\mathbb{Z}_{MN})^2\}.$$

Further, we define the center matrix $\mathbf{H}_o \triangleq (\underline{\mathbf{H}} + \bar{\mathbf{H}})/2$, which is the nominal spatially-invariant plant that will be used to design the update law.

The interval uncertainty model defined as such is a special case of the polytopic uncertainty model on $\mathbf{H}$: The set $\mathbf{H}^I$ is a compact convex matrix polytope (specifically, a hyperrectangle) with its vertices given by $\mathbf{H}^V$; i.e. $\mathbf{H}^I$ is the set of all convex combinations of the elements of $\mathbf{H}^V$.

Remark 2. *The uncertainty description $\underline{\mathbf{H}} \preccurlyeq \mathbf{H} \preccurlyeq \bar{\mathbf{H}}$ is easier to work with, but conservative in the sense that those columns of $\mathbf{H}$ corresponding to the zero-padded coordinates need not be uncertain.*

B. Nominal Stability and Convergence

As the readers might expect, the nominal stability and convergence properties of the system extends trivially from temporal ILC. Given the update law

$$\mathbf{f}_{j+1} = \mathbf{L_f}\mathbf{f}_j + \mathbf{L_e}(\mathbf{g}_d - \mathbf{g}_j), \quad \forall j \in \mathbb{N}, \tag{4}$$

the nominal system is

1) asymptotically stable if and only if $\mathbf{L_f} - \mathbf{L_e}\mathbf{H}_o$ is Schur, and
2) monotonically convergent in a given norm $\|.\|$ if and only if the corresponding induced norm satisfies

$$\gamma_o \triangleq \|\mathbf{L_f} - \mathbf{L_e}\mathbf{H}_o\| < 1.$$

Here, monotonic convergence refers to that of the input vector; that is, the condition on γ_o guarantees the existence of a fixed point $\mathbf{f}_\infty$ such that $\left\|\mathbf{f}_\infty - \mathbf{f}_{j+1}\right\| \leq \gamma_o \left\|\mathbf{f}_\infty - \mathbf{f}_j\right\|$ for all $j \in \mathbb{N}$.

One special case is when $\mathbf{L_f}, \mathbf{L_e} \in \mathrm{Circ}(M, N)$, and thus the 2-norm monotonic convergence criterion can be expressed in the frequency domain as

$$\left\|L_f(u,v) - L_e(u,v) \circ H_o(u,v)\right\|_\infty < 1.$$

We also note that the majority of existing design techniques for linear discrete-time ILC can be directly extended to the spatial case as most methods assume little more than linearity and do not explicitly account for causality.

C. The Robust Monotonic Convergence Problem

In general, the problem of ensuring asymptotic stability for all $\mathbf{H} \in \mathbf{H}^I$ is a difficult problem. If the plant matrix $\mathbf{H}$ is allowed to be iteration varying, then robust stability necessitates checking whether the joint spectral radius is strictly less than one, which has been conjectured to be an undecidable problem [22]. As our assumption is that of interval uncertain dynamics, we will focus on the easier (but practically more desirable) problem of guaranteeing monotonic convergence for all $\mathbf{H} \in \mathbf{H}^I$. The robust monotonic convergence problem is that of ensuring

$$\max_{\mathbf{H} \in \mathbf{H}^I} \|\mathbf{L_f} - \mathbf{L_e}\mathbf{H}\| < 1$$

for a given induced norm $\|.\|$. The following stability test is a generalization of Theorems 4.12 and 4.13 of [20], which shows that it suffices to check a finite set of matrices to ensure the robust contraction condition.

Proposition 1. *For any matrices $\mathbf{L_f}, \mathbf{L_e}$ and any norm $\|.\|$, not necessarily induced, the following is true:*

$$\max_{\mathbf{H} \in \mathbf{H}^I} \|\mathbf{L_f} - \mathbf{L_e}\mathbf{H}\| = \max_{\mathbf{H} \in \mathbf{H}^V} \|\mathbf{L_f} - \mathbf{L_e}\mathbf{H}\| \tag{5}$$

Proposition 1 generalizes Theorems 4.12 and 4.13 of [20] along several directions. Mainly, it shows that the findings of these results hold for 2D (spatially-varying, "noncausal") systems, regardless of the choice of norm. Of course, it is possible to find efficient tests that require fewer number of computations for specific norms. We are primarily interested in the *induced norm* cases since these correspond to robust monotonic convergence; one example for such a test is given in Appendix B. Another example is the method of computing the largest singular value of interval matrices presented in [23], which can be used to estimate $\max_{\mathbf{H} \in \mathbf{H}^I} \|\mathbf{L_f} - \mathbf{L_e}\mathbf{H}\|_2$ and ensure robustness in the 2-norm topology.[3]

Remark 3. *Proposition 1 extends directly to more general polytopic uncertainty models on the plant matrix $\mathbf{H}$, as can be seen in the proof in Appendix A. More specifically, since the proof solely invokes the polytopic structure of $\mathbf{H}^I$, with no reference to the fact that it is a set of interval matrices, given any compact convex polytope $\widehat{\mathbf{H}} \subset \mathbb{R}^{MN \times MN}$ with vertex set $\widehat{\mathbf{H}}^V \subset \widehat{\mathbf{H}}$, it follows that*

$$\max_{\mathbf{H} \in \widehat{\mathbf{H}}} \|\mathbf{L_f} - \mathbf{L_e}\mathbf{H}\| = \max_{\mathbf{H} \in \widehat{\mathbf{H}}^V} \|\mathbf{L_f} - \mathbf{L_e}\mathbf{H}\|.$$

The induced norm robust monotonic convergence tests, while useful, do not give us much insight on the design of the matrices $\mathbf{L_f}$ and $\mathbf{L_e}$. Rather, we will concentrate on the problem of quantifying the allowable perturbations on the nominal plant such that asymptotic stability and monotonic convergence are preserved. These problems will be resolved in the following sections. However, before proceeding, a fundamental issue that arises in the context of AM must be addressed.

D. Constrained Systems

Up until this point, we have ignored the fact that the SILC in the context of AM is in essence a constrained control problem. Namely, we have the following *elementwise* constraints:

1) **The sign constraint:** As the name additive manufacturing suggests, one can only add material and not subtract. This can be expressed as nonnegativity constraints on the input and the impulse response; $\mathbf{f}_j \succcurlyeq 0$ and $\bar{\mathbf{H}} \succcurlyeq \mathbf{H} \succcurlyeq \underline{\mathbf{H}} \succcurlyeq 0$.
2) **The zero-padding constraint:** Certain elements of the input vector are constrained to be zero due to the zero-padding assumption.
3) **Actuator saturation constraint:** The input is constrained by an upper (and possibly a lower) bound that is invariant in space.

Observe that when $\mathbf{f}_j \succcurlyeq 0$, it is necessary and sufficient for the plant matrix to satisfy the constraint $\mathbf{H} \succcurlyeq 0$ so that the output $\mathbf{g}_j = \mathbf{H}\mathbf{f}_j$ is elementwise nonnegative. Indeed, the inequality $\mathbf{g}_j \succcurlyeq 0$ is obvious when both $\mathbf{H}$ and $\mathbf{f}_j$ are elementwise nonnegative. On the other hand, if $\mathbf{H}$ has a negative element in row i, and $\mathbf{f}_j$ is selected as the standard basis vector pointing in the direction of the i-th axis of $\mathbb{R}^{MN}$ (that is, every component of $\mathbf{f}_j$ is zero, save for the i-th component, which is one), then $\mathbf{g}_j$ has a positive component.

Constrained ILC is a problem that has been studied in various works [24]–[29]. We will not discuss the constrained control problem in detail and instead analyze the linear approximation. To verify the validity of this approximation, we rely on a general input-constrained system of the form

$$\mathbf{g}_j = \mathbf{H}\mathbf{f}_j + \mathbf{d} \quad \mathbf{f}_j \in \mathbf{f}^I \tag{6}$$

[3]Note that this estimate is not necessarily exact: while $\|\mathbf{L_f} - \mathbf{L_e}\mathbf{H}^I\|$ is a compact convex polytope (see the proof of Proposition 1), it is not necessarily an interval matrix.

for all $j \in \mathbb{N}$, where $\mathbf{d}$ is an iteration-invariant term that includes the combined effect of initial conditions and perturbations, and

$$\mathbf{f}^I \triangleq [\underline{a}_1, \bar{a}_1] \times [\underline{a}_2, \bar{a}_2] \times [\underline{a}_{MN}, \bar{a}_{MN}] \subset \mathbb{R}^{MN} \tag{7}$$

for some vectors

$$\underline{a} \triangleq (\underline{a}_1, \underline{a}_2, \ldots, \underline{a}_{MN}),$$
$$\bar{a} \triangleq (\bar{a}_1, \bar{a}_2, \ldots, \bar{a}_{MN}),$$

satisfying $\underline{a} \preccurlyeq \bar{a}$. Here, $\underline{a}$ and $\bar{a}$ are meant to represent and generalize the elementwise constraints on the input $\mathbf{f}_j$, and the notation $\mathbf{f}^I$ refers to the interval structure in (7). The constraint $\mathbf{H} \succcurlyeq 0$ is omitted in (6) since it is a specific case of the model described by (6)-(7), and this property is not needed for the subsequent proposition discussing monotonic convergence with constraints. For the update law, it is assumed that

$$\mathbf{f}_{j+1} = \mathrm{sat}_{\bar{a}}^{\underline{a}}(\mathbf{L_f}\mathbf{f}_j + \mathbf{L_e}(\mathbf{g}_d - \mathbf{g}_j)) \quad \forall j \in \mathbb{N}, \tag{8}$$

where $\mathrm{sat}_{\bar{a}}^{\underline{a}}$ is a vector saturation function acting in an elementwise fashion, defined in the proof of Proposition 2. The following result states that the monotonic convergence of the unconstrained system is a sufficient condition for the monotonic convergence of the input-constrained system.

Proposition 2. *For a given $\mathfrak{p}$-norm $\|.\|_{\mathfrak{p}}$, where $\mathfrak{p} \in [1, \infty]$, if the contraction condition*

$$\max_{\mathbf{H}\in\mathbf{H}^I} \|\mathbf{L_f} - \mathbf{L_e}\mathbf{H}\|_{\mathfrak{p}} = \max_{\mathbf{H}\in\mathbf{H}^V} \|\mathbf{L_f} - \mathbf{L_e}\mathbf{H}\|_{\mathfrak{p}} \leq \gamma < 1$$

holds, the input of the constrained system (6)-(8) *is monotonically convergent with rate γ in the $\mathfrak{p}$-norm topology for any $\mathbf{H} \in \mathbf{H}^I$.*

Remark 4. *For the case of $\mathbf{L_f} = \mathbf{I}$, it is common to analyze monotonic convergence in the error vector, which necessitates that $\mathbf{I} - \mathbf{L_e}\mathbf{H}$ is a contraction for all $\mathbf{H} \in \mathbf{H}^I$. Unfortunately, this does not imply monotonic convergence of the error for the constrained case (for example, see algorithm 2 of [24]), hence our motivation for concentrating on input monotonic convergence.*

Remark 5. *As stated in the introduction, the layer-by-layer dynamics arising in many AM applications are best represented in the repetitive process framework. An accurate repetitive process model for such applications should consider constraints, nonlinearities, dependence on independent variables other than spatial coordinates (x, y) and time t, time-varying factors, delays, for both the in-layer and layer-to-layer dynamics. As we focus on the dynamics of a single layer, based on a scenario in which the build quality of a single-layer product is improved via ILC, and the single-layer dynamics of the application example of Section VII can be represented by the linear spatially-varying model presented in this section, these more complex models will not be investigated. This approach is based on the implicit assumption that as in differential/difference equations, a linear model is valid around the equilibrium. A similar linearization-based approach for AM systems has been explored in [30]. A rigorous basis for linearization for a class of repetitive processes is presented in [31].*

IV. Interval Stability Radii using the DFT-based Lyapunov Equation

In this section, we present the notion of interval stability radii in SILC as it relates to our problem. As in multivariable linear control, the radii will define the largest ball centered around the nominal system in a given induced norm topology so that asymptotic stability, or monotonic convergence, is preserved. The idea is to ensure a linear matrix inequality of the form

$$(\mathbf{L_f} - \mathbf{L_e}\mathbf{H})^*\mathbf{P}(\mathbf{L_f} - \mathbf{L_e}\mathbf{H}) - \mathbf{P} < 0 \quad \forall\, \mathbf{H} \in \mathbf{H}^I,$$

based on the Lyapunov equation for the nominal plant, as this implies that the eigenvalues of $\mathbf{L_f} - \mathbf{L_e}\mathbf{H}$ are inside the unit disk for all $\mathbf{H} \in \mathbf{H}^I$.

We begin by defining the radius matrix $\mathbf{H}_r \triangleq (\bar{\mathbf{H}} - \underline{\mathbf{H}})/2$, which is used to define an additive perturbation to the center matrix to quantify robustness via the Lyapunov equation. From this point onward, we will assume that $\mathbf{L_f}$ and $\mathbf{L_e}$ are in $\mathrm{Circ}(M, N)$.

A. Quantification of the Uncertainty

The size of the interval uncertainty set, as defined by the radius matrix $\mathbf{H}_r$, can be quantified equivalently by the induced 1- or infinity norms. It is natural to use the 1- or the infinity norm of the uncertainty as these are defined to be the maximum absolute row or column sums. Interestingly, due to the symmetry of the uncertainty set about zero for each coordinate, the induced 2-norm quantification of the uncertainty is equivalent to these as shown below.

Proposition 3. *For any $\mathfrak{p} \in \{1, 2, \infty\}$ the following is true:*

$$\max_{-\mathbf{H}_r \preccurlyeq \mathbf{H}_\delta \preccurlyeq \mathbf{H}_r} \|\mathbf{H}_\delta\|_{\mathfrak{p}} = \|\mathbf{H}_r\|_1 = \|\mathbf{H}_r\|_\infty = \|\mathbf{H}_r\|_2 .$$

Hence, we define $r_{\mathrm{int}} \triangleq \|\mathbf{H}_r\|_1$ as the equivalent quantifier of the size of the uncertainty set over the induced 1-, 2-, and infinity norms. Note that r_{int} also equals the l_1 norm of $(\bar{h}(x, y) - \underline{h}(x, y))/2$.

B. DFT Solution of the Lyapunov Equation

Recall that the nominal asymptotic stability condition in the supervector framework dictates that the eigenvalues of the matrix $\mathbf{T}_o \triangleq \mathbf{L_f} - \mathbf{L_e}\mathbf{H}_o$ are in the open unit disk. Consequently, the nominal asymptotic stability condition can be equivalently represented by the discrete Lyapunov equation:

$$\mathcal{L}(\mathbf{T}_o, \mathbf{P}) \triangleq \mathbf{T}_o^*\mathbf{P}\mathbf{T}_o - \mathbf{P} = -\mathbf{I}, \tag{9}$$

where $\mathbf{P}$ is symmetric and positive definite. Due to our assumption that the update law matrices $\mathbf{L_f}, \mathbf{L_e} \in \mathrm{Circ}(M, N)$, the equation can be solved algebraically via the 2D DFT, leading to

$$P(u, v) = \frac{1}{1 - |T_o(u, v)|^2} \quad \forall (u, v) \in \mathbb{Z}_M \times \mathbb{Z}_N. \tag{10}$$

Note that the above is well defined if $\mathbf{T}_o$ is Schur.

The advantage of the above identity is that the Lyapunov equation can be solved efficiently for large sample sizes via

the DFT. Moreover, if the plant uncertainty is assumed to be spatially-invariant, frequency-based methods can be employed to robustly shape the "loop". We refer the interested readers to the results of Chapter 5 of [20], which can easily be specialized to limit uncertainties to BCCB matrices.

C. Interval Asymptotic-Stability Radius

The interval asymptotic-stability radius estimate $r_{\max}^{\text{asymp}}$ is a measure of the allowable interval uncertainty such that asymptotic stability is preserved. The estimate can be computed for any given induced matrix norm $\|.\|$ such that if

$$\max_{-\mathbf{H}_r \preccurlyeq \mathbf{H}_\delta \preccurlyeq \mathbf{H}_r} \|\mathbf{H}_\delta\| < r_{\max}^{\text{asymp}},$$

the ILC system is robustly asymptotically stable [20].

The quantity $r_{\max}^{\text{asymp}}$ is only an estimate of the allowable perturbations to the plant and could therefore be conservative. As we have shown that the radius uncertainty can be equivalently quantified in terms of the induced 1-, 2-, and infinity norms, a possible approach to find tighter bounds is to compute the radius for these three norms and take the maximum of these as the allowable interval uncertainty.[4] We will instead concentrate on the 2-norm based radius since it can be efficiently computed in the frequency domain. Another advantage to this computation is that the maximization of the radius, or other problems relating to optimality, is a much more straightforward problem in the frequency domain. Using the solution of the Lyapunov equation, the definition of the estimate $r_{\max}^{\text{asymp}}$ follows with trivial substitutions to the proof of Theorem 5.2 of [20]:

$$\begin{aligned} r_{\max}^{\text{asymp}} &\triangleq \frac{-\|\mathbf{T}_o\|_2 + \sqrt{\|\mathbf{T}_o\|_2^2 + \|\mathbf{P}\|_2^{-1}}}{\|\mathbf{L_e}\|_2} \\ &= \frac{-\left\|T_o(u,v)\right\|_\infty + \sqrt{\left\|T_o(u,v)\right\|_\infty^2 + \left\|P(u,v)\right\|_\infty^{-1}}}{\left\|L_e(u,v)\right\|_\infty} \\ &= \frac{1-\left\|T_o(u,v)\right\|_\infty}{\left\|L_e(u,v)\right\|_\infty}, \end{aligned}$$

where the second equality follows from (10), as

$$\left\|P(u,v)\right\|_\infty = (1-\left\|T_o(u,v)\right\|_\infty^2)^{-1}.$$

D. Interval Monotonic-Convergence Radius

The concept of interval asymptotic-stability radius can be extended to define a radius of monotonic convergence. First, we define the augmented matrix

$$\mathbf{T}_o^{\text{aug}} \triangleq \begin{bmatrix} 0 & \mathbf{T}_o^* \\ \mathbf{T}_o & 0 \end{bmatrix}.$$

Note that the spectral radius of $\mathbf{T}_o^{\text{aug}}$ is equal to the maximum singular value of $\mathbf{T}_o$ as can be seen from block matrix determinant formulas. Then, the solution $\mathbf{P}^{\text{aug}}$ of the following Lyapunov equation is symmetric and positive definite, since the spectral radius and the maximum singular value of the BCCB matrix T_o are equal:

$$(\mathbf{T}_o^{\text{aug}})^* \mathbf{P}^{\text{aug}} \mathbf{T}_o^{\text{aug}} - \mathbf{P}^{\text{aug}} = -\mathbf{I}.$$

The augmented Lyapunov equation will ensure that the singular values of $\mathbf{L_f} - \mathbf{L_e}\mathbf{H}$ are strictly less than one for all $\mathbf{H} \in \mathbf{H}^I$. Thus, as opposed to the previous case, we will compute a stability radius that ensures monotonic convergence strictly in the *2-norm topology*.

Unlike the previous Lyapunov equation, it is not obvious that we can use the DFT to solve for $\mathbf{P}^{\text{aug}}$ since $\mathbf{T}_o^{\text{aug}}$ is not BCCB. However, by direct substitution, it is trivial to show that $\mathbf{P}^{\text{aug}} = \text{diag}(\mathbf{P}, \mathbf{P})$ where $\mathbf{P}$ is the inverse DFT of (10); i.e. the solution of the Lyapunov equation (9). Furthermore, we have $\|\mathbf{T}_o^{\text{aug}}\|_2 = \left\|T_o(u,v)\right\|_\infty$, and

$$\|\mathbf{P}^{\text{aug}}\|_2 = \|\mathbf{P}\|_2 = (1-\left\|T_o(u,v)\right\|_\infty^2)^{-1}.$$

As a result, the interval monotonic-convergence radius estimate $r_{\max}^{\text{mono}}$ can be given by the following formula, which turns out to be identical to the estimate $r_{\max}^{\text{asymp}}$:

$$\begin{aligned} r_{\max}^{\text{mono}} &\triangleq \frac{-\|\mathbf{T}_o^{\text{aug}}\|_2 + \sqrt{\left\|\mathbf{T}_o^{\text{aug}}\right\|_2^2 + \|\mathbf{P}^{\text{aug}}\|_2^{-1}}}{\|\mathbf{L_e}\|_2} \\ &= \frac{1-\left\|T_o(u,v)\right\|_\infty}{\left\|L_e(u,v)\right\|_\infty} = r_{\max}^{\text{asymp}}. \end{aligned} \tag{11}$$

As the two estimates are found to be equal, henceforth we will refer to them simply as the "stability-radius estimate", which will be denoted $r_{\max}$.

The identity computes a tighter lower bound on the interval monotonic convergence radius in the 2-norm topology than the one defined in Theorem 5.6 and Corollary 5.7 of [20], since $\|.\|_2 \leq \|.\|_1 = \|.\|_\infty$ for BCCB matrices. As such, we require a small modification to the proof, which is discussed in Appendix C.

Remark 6. *The readers might note that the resulting identity for $r_{\max}$ could have been computed via the triangle inequality on the perturbed system (see the convergence rate computation in the next subsection), similar to Theorem 4 of [11] and Theorem 7 of [32]. This is somewhat surprising and would not necessarily be the general case for spatially-varying update laws and/or nominal plants. Whether the Lyapunov-based methodology results in less conservative bounds is an open question.*

E. Worst-Case Convergence Rate

The condition $r_{\text{int}} < r_{\max}$ ensures that the singular values of $\mathbf{L_f} - \mathbf{L_e}\mathbf{H}$ are strictly less than one. More strongly, the bound guarantees that the set of singular values is strictly bounded away from zero. The formal argument for this is due to the compactness of $\mathbf{H}^I$. Because the transformation $\mathbf{H} \mapsto \mathbf{L_f} - \mathbf{L_e}\mathbf{H}$ is affine, it is continuous and maps $\mathbf{H}^I$ to another compact set. As a result, the proposition $\|\mathbf{L_f} - \mathbf{L_e}\mathbf{H}\|_2 < 1$ for all $\mathbf{H} \in \mathbf{H}^I$ implies

$$\gamma \triangleq \max_{\mathbf{H} \in \mathbf{H}^I} \|\mathbf{L_f} - \mathbf{L_e}\mathbf{H}\|_2 < 1.$$

[4] Recall that asymptotic stability does not depend on the choice of norm and necessitates that the spectral radius is strictly less than one.

Therefore, the worst-case convergence rate γ can be computed exactly by aid of Proposition 1. As this process requires $2^{(MN)^2}$ computations, it makes sense to rely on a simple estimate. Assume that the plant perturbation satisfies $-\mathbf{H}_r \preccurlyeq \mathbf{H}_\delta \preccurlyeq \mathbf{H}_r$. Then,

$$\begin{aligned}\left\|\mathbf{L_f} - \mathbf{L_e}(\mathbf{H}_o + \mathbf{H}_\delta)\right\|_2 &= \|\mathbf{T}_o - \mathbf{L_e}\mathbf{H}_\delta\|_2 \\ &\leq \|\mathbf{T}_o\|_2 + \|\mathbf{L_e}\|_2\|\mathbf{H}_\delta\|_2 \\ &\leq \left\|T_o(u,v)\right\|_\infty + \left\|L_e(u,v)\right\|_\infty r_{\text{int}} \\ &< 1.\end{aligned}$$

The results of this section are conveniently summarized with the following theorem:

Theorem 1. *The ILC system* (2) *with the update law* (4)*, where* $\mathbf{L_f}, \mathbf{L_e} \in \text{Circ}(M,N)$*, is robustly monotonically convergent for all* $\mathbf{H} \in \mathbf{H}^I$ *in the 2-norm topology if* $r_{\text{int}} \leq r_{\max}$*; in other words, if*

$$\|\mathbf{H}_r\|_1 \leq \frac{1 - \left\|T_o(u,v)\right\|_\infty}{\left\|L_e(u,v)\right\|_\infty}.$$

Furthermore, if $r_{\text{int}} \leq r_{\max}$*, then*

$$\gamma \triangleq \max_{\mathbf{H}\in\mathbf{H}^I} \|\mathbf{L_f} - \mathbf{L_e}\mathbf{H}\|_2 \leq \left\|T_o(u,v)\right\|_\infty + r_{\text{int}}\left\|L_e(u,v)\right\|_\infty.$$

V. On Iteration-Varying Uncertainties and Disturbances

Although we have not explicitly defined an iteration-varying plant in (1), we note that a linear ILC system is stable in the presence of iteration-varying uncertainties if the update law is robustly monotonically convergent within the uncertainty set. Furthermore, the gain of the matrix $\mathbf{L_e}$, along with the worst-case convergence rate, defines a measure of the steady-state deviations from the nominal performance in the presence of uncertainties [33]. This measure, which we denote as φ, is given by the following formula, and generally speaking, lower values of φ signifies less variation in the steady-state performance when compared to the nominal system without disturbances:

$$\begin{aligned}\varphi &= \frac{\left\|L_e(u,v)\right\|_\infty}{1 - \left(\left\|T_o(u,v)\right\|_\infty + r_{\text{int}}\left\|L_e(u,v)\right\|_\infty\right)} \\ &= (r_{\max} - r_{\text{int}})^{-1}.\end{aligned}$$

Therefore, the predictability of the system increases as the stability radius increased. However, this increase might come at the expense of nominal performance.

As compared to other methodologies in the literature, minimization of the norm-based measure we have outlined above makes more practical sense with respect to our target applications. It is practically unlikely that the spatial dynamics satisfy higher-order internal models along the iteration axis. On the other hand $\mathcal{H}_\infty$ methods yield update laws that are *computationally infeasible*, as the resulting algorithms are time-varying (for temporal systems) and have *extremely high*[5] order [20], even though it has been noted in [34] that higher-order algorithms are no more optimal than first-order algorithms when it comes to rejection of stochastic disturbances.

[5]More specifically, if n data points are collected at each trial, the resulting algorithm is n-th order.

VI. Update Law Design via the Stability Radius

In this section we discuss the optimal design of the update law with respect to the stability-radius estimate. As there is a trade-off between the estimate and nominal tracking performance, it makes sense to include the nominal steady-state error in the optimization problem.

In the case of the nominal iteration-invariant system, the limiting performance is defined by the reference-to-error transfer function $S(u,v)$, which we will refer to as the *sensitivity function* for the obvious reason:

$$S(u,v) \triangleq \frac{1 - L_f(u,v)}{1 - T_o(u,v)} \quad \forall (u,v) \in \mathbb{Z}_M \times \mathbb{Z}_N.$$

Hence, while decreasing sensitivity gains imply better tracking for nominal systems, this might come at the expense of increased steady-state variations under uncertainties.

A. Optimal Design

Based on our previous discussion, along the lines of [33], we suggest the following general optimization problem for the design of the update law matrices $L_f(u,v)$ and $L_e(u,v)$:

$$\begin{aligned}\underset{L_f(u,v),L_e(u,v)}{\text{minimize}} \quad & \mathcal{F}(r_{\max}^{-1}, \left\|S(u,v)\right\|_\infty, \gamma) \geq 0 \\ \text{subject to} \quad & \left\|S(u,v)\right\|_\infty \leq \bar{s} \leq 1, \\ & r_{\max} \geq r_{\text{int}}, \\ & \gamma \leq \bar{\gamma} < 1,\end{aligned}$$

where $\bar{s}$ is an acceptable sensitivity gain and $\bar{\gamma}$ is an acceptable convergence rate. The specifics of the cost function $\mathcal{F}$ would naturally depend on the nature of the application, such as the level of uncertainty and disturbances. Of course, it is possible to modify this problem in many ways. One obvious change is to require the constraints on the sensitivity function to be frequency-dependent. The DFT formulation is computationally advantageous in posing the ILC problem as a constrained minimization shown above, since the matrix multiplication and inversion operations encountered in the spatial domain simplify to pointwise multiplication and division. As such, one might also take the arguments to the optimization problem to be frequency-dependent transfer functions.

B. Feasibility of Perfect Tracking under Uncertainties

We discuss the special case of $\mathbf{L_f} = \mathbf{I}$, which is the widely-known necessary and sufficient condition for perfect tracking for iteration-invariant systems, derived from the internal model principle, when (5) holds. Since (11) describes the estimates compactly in the frequency domain, the optimization problem of maximizing the stability radius estimate can be solved by fixing the frequency $(u,v) \in \mathbb{Z}_M \times \mathbb{Z}_N$, and studying the auxiliary problem of maximizing the quantity $(1 - |T_o(u,v)|)/|L_e(u,v)|$. First, note that the identity

$$|L_e(u,v)| = \frac{|L_e(u,v)H_o(u,v)|}{|H_o(u,v)|} \quad \forall (u,v) \in \mathbb{Z}_M \times \mathbb{Z}_N$$

implies that the minimization of $|L_e(u,v)|$ is equivalent to the minimization of $|L_e(u,v)H_o(u,v)|$ for all $(u,v) \in \mathbb{Z}_M \times \mathbb{Z}_N$.

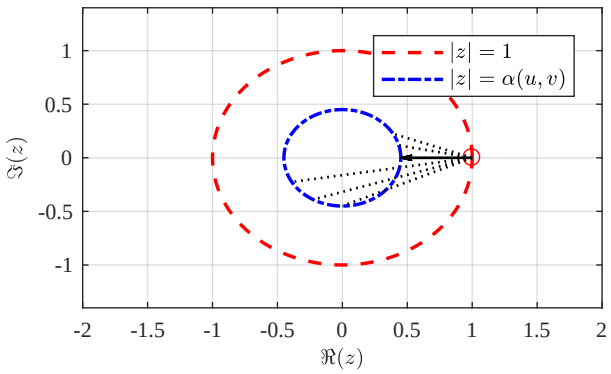

Fig. 1: Illustration of the auxiliary optimization problem for stability-radius maximization for the specific case $\mathbf{L_f} = \mathbf{I}$. Given $|1 - L_e(u,v)H_o(u,v)| = \alpha(u,v)$, the complex number $L_e(u,v)H_o(u,v)$ with the minimum magnitude is the outwards normal to the $\alpha(u,v)$ circle at $\alpha(u,v)$, with magnitude $1 - \alpha(u,v)$. The solid black arrow is the optimal vector $-L_e(u,v)H_o(u,v)$.

Given the constraint

$$|T_o(u,v)| = |1 - L_e(u,v)H_o(u,v)| \\ = \alpha(u,v) \in \left[0, \left\|T_o(u,v)\right\|_\infty\right] \quad \forall u \in \mathbb{Z}_M, v \in \mathbb{Z}_N,$$

where $\left\|T_o(u,v)\right\|_\infty < 1$, the minimizer of $|L_e(u,v)H_o(u,v)|$ is the shortest distance vector from the $\alpha(u,v)$ circle centered at the origin to 1 (see Fig. 1), which requires

$$L_e(u,v) = (1 - \alpha(u,v))/H_o(u,v) \quad \forall (u,v) \in \mathbb{Z}_M \times \mathbb{Z}_N.$$

Now we have,

$$|L_e(u,v)| = \frac{1 - \alpha(u,v)}{|H_o(u,v)|} \\ \geq \frac{1 - \left\|T_o(u,v)\right\|_\infty}{|H_o(u,v)|} \quad \forall (u,v) \in \mathbb{Z}_M \times \mathbb{Z}_N.$$

Hence, if $\alpha(u,v) = \left\|T_o(u,v)\right\|_\infty$ for all $(u,v) \in \mathbb{Z}_M \times \mathbb{Z}_N$, it follows that

$$\left\|L_e(u,v)\right\|_\infty = (1 - \left\|T_o(u,v)\right\|_\infty) \left(\min_{\substack{u \in \mathbb{Z}_M \\ v \in \mathbb{Z}_N}} |H(u,v)| \right)^{-1}.$$

Thus, the stability-radius estimate is equal to the minimum modulus of $H_o(u,v)$, the minimum eigenvalue perturbation to $\mathbf{H}_o$ that results in singularity:

$$r_{\max} = \min_{\substack{u \in \mathbb{Z}_M \\ v \in \mathbb{Z}_N}} |H_o(u,v)|.$$

In other words, the estimate is given by the $\mathcal{H}_\infty$ norm of the inverse of $H(u,v)$. Therefore, perfect tracking is a feasible objective for the uncertain system if the uncertainty r_{int} is lower than the gain of the inverse system;

$$r_{\text{int}} = \|\mathbf{H}_r\|_1 < \min_{\substack{u \in \mathbb{Z}_M \\ v \in \mathbb{Z}_N}} |H_o(u,v)|,$$

as discussed for the 1D temporal case in [35].

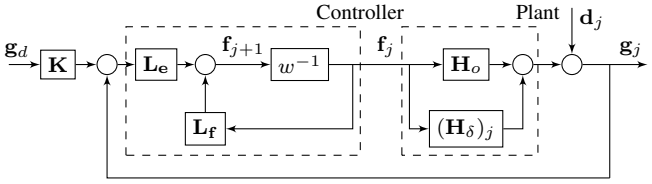

Fig. 2: Precompensation in the iteration domain: Since ILC can be interpreted as feedback control in the iteration domain, it is easy to conclude aggressive learning might amplify disturbances. When $\mathbf{L_f} \neq \mathbf{I}$, the precompensator $\mathbf{K}$ can be used to partially recover the tracking performance. Here, w^{-1} represents the trial-delay operator; $(\mathbf{H}_\delta)_j$ is the plant perturbation and $\mathbf{d}_j$ is a term that represents disturbances, noise, and the effect of initial conditions, both iteration-varying.

C. When Perfect Tracking is not Feasible or Desirable

When the additive uncertainty is high in magnitude (Section VI-B), and/or the system is subject to iteration-varying effects, perfect tracking is an infeasible objective. Depending on the level of uncertainty, minimizing the measure φ (in other words, the *relative error*) can be taken as an objective of primary importance over the steady-state (in other words, the absolute error) performance [33]. In the case of manufacturing applications, precision is arguably more important than accuracy, and repeatable errors could be preferred.[6] If perfect tracking is infeasible or undesirable, *precompensation in the iteration domain* (see Fig. 2) can be used as an ad hoc fix to recover[7] tracking performance [33]. While this precompensator can be constructed using empirical data, a simple choice is given by inverting the nominal "complementary sensitivity function", $1 - S(u,v)$ for all $(u,v)(u,v) \in \mathbb{Z}_M \times \mathbb{Z}_N$ (i.e., the steady-state reference-to-output transfer function):

$$K_o(u,v) = \frac{L_e(u,v)H_o(u,v)}{1 - T_o(u,v)} \quad \forall (u,v) \in \mathbb{Z}_M \times \mathbb{Z}_N.$$

VII. Case Study: Norm-Optimal SILC Applied to Electrohydrodynamic Jet Printing

This section presents a case study of a norm-optimal SILC (NO-SILC) update law, designed using the RMC criterion in Theorem 1 to predict stability and practical convergence in the presence of spatially/iteration-varying uncertainties, applied to the microscale-AM process electrohydrodynamic jet (e-jet) printing. Here, we provide cursory information on the e-jet system with integrated atomic force microscope (AFM) sensing; the complete system description can be found in [36].

A. System Model

E-jet printing is a microscale-AM process that can achieve a smaller resolution than ink-jet printing and can use a diverse

[6]Another valid reason for this approach is the difficulty or impossibility of applying feedback control to reduce the effect of nonrepetitive disturbances for additive manufacturing applications.

[7]This is akin to the fact that precompensation can be used to recover DC gains of linear systems under state-feedback.

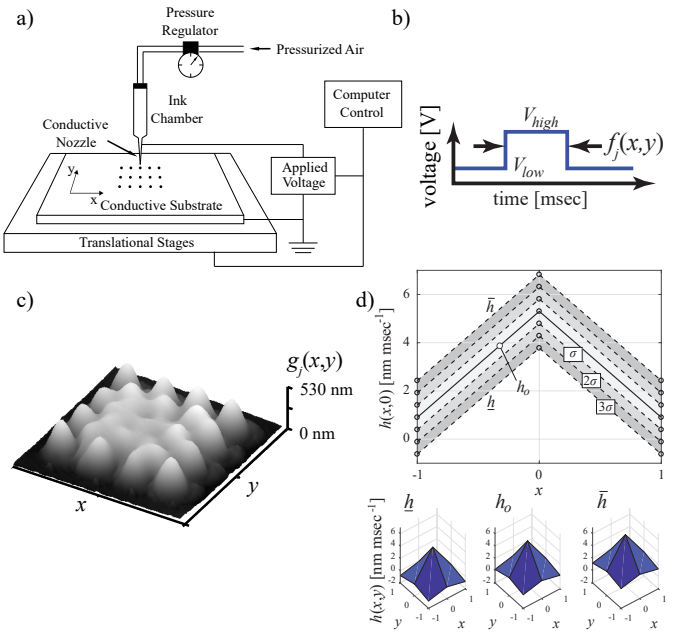

Fig. 3: E-jet system and systems description. a) Components of a standard e-jet printing system. b) The input is a voltage pulse applied at spatial coordinate (x, y) with pulse width $f_j\,(x, y)$. c) AFM scan of the output $g_j(x, y)$, which is the steady-state topography of the deposited material at discrete coordinates (x, y). d) Identified nominal response h_o, along with the upper and lower bounds of the interval model, $\underline{h}$ and $\bar{h}$, respectively. The cross sections of the impulse response models at $y = 0$ are shown for the σ, 2σ, and 3σ cases for $\underline{h}$ and $\bar{h}$, along with a surface plot illustrating the 2σ case.

array of functional materials [37]. The standard e-jet printing system consists of an ink chamber, back-pressure source, a conductive nozzle, a conductive substrate, high-voltage power supply, and translational stages (Fig. 3a). In the printing mode used in our case study, the electrical potential between the substrate and the nozzle is pulsed from V_{low} to V_{high}. The electric field draws the ink into a cone, which is then ejected as a single drop from the tip of the cone. Here, the input to the system is the width of the voltage pulse $f_j\,(x, y)$ applied at coordinate (x, y). By coordinating the position of the nozzle (x, y) and input $f_j\,(x, y)$, complex microscale structures can be fabricated. The system output $g_j\,(x, y)$ is the topography of the fabricated structure (Fig. 3c). This particular e-jet system has an integrated atomic force microscope (AFM) to measure the part topography at each SILC iteration.

In lieu of using the solution of the PDE representing the dynamics of material accumulation in e-jet printing, with assumed and experimentally determined parameters, we use the system identification method described in [38] to compute the 3×3 spatial impulse response at steady-state (Fig. 3d). Our system identification method permits us to compute the nominal response h_o. To observe how the RMC criterion is affected by differing levels of uncertainty, we consider three different cases for the impulse response bounds and define $\underline{h} = h_o - a\sigma\mathbf{1}(3,3)$ and $\bar{h} = h_o + a\sigma\mathbf{1}(3,3)$, where σ is the standard deviation of the identified nominal impulse response, and $\mathbf{1}(3,3)$ is a 3×3 matrix of 1's, bounding 68.2%, 95.4%, and 99.6% of the potential system responses for the case of $a = 1$, $a = 2$, and $a = 3$, respectively.[8] Here, the functions $\underline{h}$ and $\bar{h}$ represent the bounds on the distribution of the material added to the substrate in response to a unit input. For example, when a unit voltage pulse is applied at coordinate (x, y), the material height at coordinate $(x + 1, y)$ will be between $\underline{h}(1, 0)$ and $\bar{h}(1, 0)$. Also note that e-jet is a naturally constrained system (the process can only add material and the pulse width $f_j(x, y)$ can only be positive) subject to high levels of iteration-varying uncertainties, in particular due to the difficulty of modeling the complex process physics at the microscale.

B. Application of the RMC Criterion to Norm-Optimal SILC

RMC is evaluated for NO-SILC update law designs. The NO-SILC update laws considered here aim to minimize the frequency-domain objective function

$$\mathcal{J} = qE^*_{j+1} \circ E_{j+1}(u, v) + sF^*_{j+1} \circ F_{j+1}(u, v) + r\left(F_{j+1} - F_j\right)^* \circ \left(F_{j+1} - F_j\right)(u, v)$$

at every iteration, where q, s, and r are real scalars that penalize the error, the input, and the change in input with respect to iteration, respectively. As shown in [12], the learning filters

$$L_f(u, v) = \frac{rI + qH^*_o \circ H_o}{qH^*_o \circ H_o + sI + rI}(u, v)$$
$$L_e(u, v) = \frac{qH^*_o}{qH^*_o \circ H_o + sI + rI}(u, v),$$

minimize the objective function $\mathcal{J}$.

The RMC criterion described in Theorem 1 is evaluated over a range of NO-SILC designs corresponding to the parameters $q = 10^0$, $r \in \left[10^{-10}, 10^{10}\right]$, and $s \in \left[10^{-10}, 10^{10}\right]$. Results corresponding to the σ, 2σ, and 3σ cases for the impulse response bounds $\underline{h}$ and $\bar{h}$ are presented in Fig. 4a. For each case, there is a clear demarcation line along the s design space axis where the RMC criterion changes from satisfied to not satisfied.

C. Experimental Study

Update laws designed using NO-SILC are applied to the e-jet/AFM metrology system. Details of the experiment can be found in [39]. The NO-SILC designs are superimposed on the RMC evaluation map in Fig. 4a. Three of the experimentally tested NO-SILC designs satisfy the RMC criterion in Theorem 1 (for the case of σ for $\underline{h}$ and $\bar{h}$), which provides a sufficient condition for monotonic (for iteration-invariant systems) and practical (for iteration-varying systems) convergence. The six designs that are logarithmically near the RMC boundary exhibit an iteration-domain response that dithers around a converged value, as can be seen in Fig. 4b. However, the design corresponding to $q = 1$, $r = 10^{-2}$, and $s = 10^{-4}$, which is distant from the boundary, exhibits an iteration-domain

[8]The identification method in [38] leads to a formulation such that each coordinate of the impulse response has the same standard deviation.

response in which the 2-norm of the error steadily increases after approximately the 12-th iteration. The 2-norm of the input signal increases with iteration as well (data not shown). In brief, the RMC criterion provides a useful guideline for an NO-SILC design to attain a practically convergent iteration-domain response in the presence of iteration-varying effects, as discussed in Section V.

It should be emphasized again that the RMC criterion in Theorem 1 is only a sufficient conditions, and a less conservative design procedure can rely on Proposition 1 at the expense of increased computational burden. A possible design procedure can use the equality in (5) in a nonlinear program as in Section VI-A to yield more reliable estimates. It is also important to note that the conservativeness of the RMC criterion depends on the accuracy of the impulse response bounds. The identification procedure used to estimate the bounds $\underline{h}$ and $\bar{h}$ in this study yields a similar statistical distribution for each coordinate of the impulse response and leads to a lower bound $\underline{h}$ which is negative at the boundary–see Fig. 3d for the case of 3σ. Research into system identification methods for spatial systems is required to define precise bounds $\underline{h}$ and $\bar{h}$, which is a challenging problem due to the nature of AM applications, and the high experimental cost when compared to the other applications in the temporal domain.

VIII. Conclusion

In this paper, we investigated an extension of the spatial iterative learning control (SILC) framework and analysis introduced in [12] to understand SILC for spatially-varying and uncertain plants. Our analysis treats spatial variations as interval uncertainties with spatially-invariant bounds, to preserve the computational efficiency in the frequency domain afforded to spatially-invariant 2D systems. Computational efficiency is particularly important to the target application of AM, which often uses spatially-distributed sensing and thus creates large datasets ($MN > 10^4$). The main contribution is the definition of the RMC criterion for interval uncertain spatial systems in the frequency domain. The utility of the RMC criterion as a useful guideline to predict stability and practical convergence of SILC in the presence of spatially/iteration-varying uncertainties was demonstrated experimentally on a microscale additive manufacturing system with spatial dynamics.

The frequency-domain analysis of RMC sets the stage for future theoretical investigations. For instance, here we defined SILC in the 2D spatial domain; however, AM applications are often spatially 3D (for example, due to heat transfer) and some AM tools, such as powder bed fusion, have important dynamics in the temporal domain. Naturally, new theory will be required to expand the analysis dimensions; we emphasize that as the number of dimensions expands, computationally-efficient tools, such as the frequency-domain analysis presented here, are even more important. Lastly, AM processes have innate layer-to-layer dynamics [30], which can be formalized as repetitive process with in-layer dynamics defined on the 2D spatial domain; new theory in the form of higher-order SILC analyses will be required to understand the layer-to-layer problem.

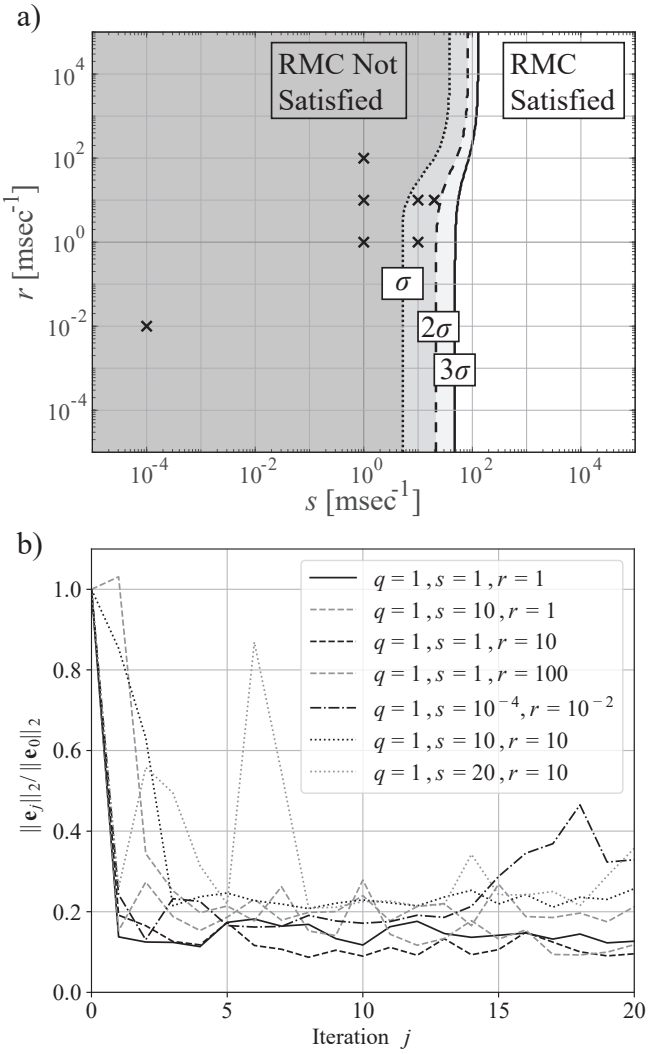

Fig. 4: Study of the RMC criterion for an array of NO-SILC designs. a) Design space in which the RMC Criterion is satisfied. Only the range $r \in \left[10^{-5}, 10^{5}\right]$, and $s \in \left[10^{-5}, 10^{5}\right]$ is shown for clarity. Cross markers denote the NO-SILC designs tested in the experiments. The RMC Criterion boundary is dependent on the estimate of $\underline{h}$ and $\bar{h}$. b) Normalized error-norm plots from experiments of seven NO-SILC designs.

Appendix A
Proofs of the Propositions

Proof of Proposition 1. It is well known that the maximum of a convex function on a compact convex polytope occurs at one of its vertices. Now, the affine transformation $\mathbf{H} \mapsto \mathbf{L_f} - \mathbf{L_e}\mathbf{H}$ maps $\mathbf{H}^I$ to another compact convex matrix polytope. Moreover, because affine transformations map vertices to vertices, the set of vertices of $\mathbf{L_f} - \mathbf{L_e}(\mathbf{H}^I)$ is precisely the set $\mathbf{L_f} - \mathbf{L_e}(\mathbf{H}^V)$. Since every norm is a convex function, we conclude $\left(\arg\max_{\mathbf{H}\in\mathbf{H}^I} \mathbf{L_f} - \mathbf{L_e}\mathbf{H}\right) \cap \mathbf{H}^V$ is nonempty. □

Proof of Proposition 2. Given $\underline{a}, \bar{a} \in \mathbb{R}^{MN}$, define the vector saturation function $\mathrm{sat}_{\bar{a}}^{\underline{a}} : \mathbb{R}^{MN} \to \mathbb{R}^{MN}$ so that

$$\mathrm{sat}_{\underline{a}}^{\bar{a}}(\mathbf{f}) = (\mathrm{sat}_{\bar{a}_1}^{\underline{a}_1}(f_1), \mathrm{sat}_{\bar{a}_2}^{\underline{a}_2}(f_2), \ldots, \mathrm{sat}_{\bar{a}_{MN}}^{\underline{a}_{MN}}(f_{MN}))$$

for any $\mathbf{f} \triangleq (f_1, f_2, \ldots, f_{MN}) \in \mathbb{R}^{MN}$, where

$$\mathrm{sat}_{\underline{a}_i}^{\bar{a}_i}(f_i) \triangleq \begin{cases} \underline{a}_i, & \text{if } f_i < \underline{a}_i \\ f_i, & \text{if } \underline{a}_i \leq f_i \leq \bar{a}_i \\ \bar{a}_i, & \text{if } f_i > \bar{a}_i \end{cases}$$

for every $i = \{1, 2, \ldots, MN\}$. It is straightforward to check that the vector saturation function is Lipschitz continuous with Lipchitz constant 1 in any $\mathfrak{p}$-norm topology, with $\mathfrak{p} \in [1, \infty]$. Next, define the function Ψ such that

$$\Psi(\mathbf{f}_j) = (\mathbf{L_f} - \mathbf{L_e}\mathbf{H})\mathbf{f}_j + \mathbf{L_e}\mathbf{d}.$$

The operator Ψ maps the input $\mathbf{f}_j$ to the input $\mathbf{f}_{j+1}$ in the unconstrained case; cascading Ψ with the saturation function recovers the true dynamics. Now for arbitrary $\mathbf{f}, \mathbf{g} \in \mathbb{R}^{MN}$

$$\begin{aligned} \left\| \mathrm{sat}_{\underline{a}}^{\bar{a}}(\Psi(\mathbf{f})) - \mathrm{sat}_{\underline{a}}^{\bar{a}}(\Psi(\mathbf{g})) \right\|_{\mathfrak{p}} &\leq \left\| \Psi(\mathbf{f}) - \Psi(\mathbf{g}) \right\|_{\mathfrak{p}} \\ &= \left\| (\mathbf{L_f} - \mathbf{L_e}\mathbf{H})(\mathbf{f} - \mathbf{g}) \right\|_{\mathfrak{p}} \\ &\leq \gamma \|\mathbf{f} - \mathbf{g}\|_{\mathfrak{p}}, \end{aligned}$$

hence we have a contraction with Lipschitz constant γ. □

Proof of Proposition 3. The equality $\|\mathbf{H}_r\|_1 = \|\mathbf{H}_r\|_\infty$ follows from the definition of BCCB matrices as discussed in Section II. Also note that we have the property $\|\mathbf{H}_r\|_2 \leq \|\mathbf{H}_r\|_\infty$ from the same section. The equality between the two can be verified by noting that the vector of ones is an eigenvector of $\mathbf{H}_r$ from circulant symmetry and entrywise nonnegativity; $\mathbf{H}_r \succcurlyeq 0$. Since the corresponding eigenvalue is $\|\mathbf{H}_r\|_\infty$, we conclude $\|\mathbf{H}_r\|_2 \geq \|\mathbf{H}_r\|_\infty$ and thus $\|\mathbf{H}_r\|_2 = \|\mathbf{H}_r\|_\infty$.

From Proposition 1, we know that the norm will be maximized at a vertex of the set given by $-\mathbf{H}_r \preccurlyeq \mathbf{H}_\delta \preccurlyeq \mathbf{H}_r$. Then, it is easy to check that the norm maximization of the 1- and infinity norms are equivalent due to the BCCB structure of the interval, and $\mathbf{H}_r$ is a maximizer. For the 2-norm case, the results of [23] (alternatively, Appendix B of [20]) can be invoked to see that $\mathbf{H}_r$ is a maximizer, thereby completing the proof. □

Appendix B
Example Stability Test

Below we show that it suffices to consider spatially-invariant plants to check robust monotonic convergence in the 1-norm topology. If $\mathbf{L_f}, \mathbf{L_e} \in \mathrm{Circ}(M, N)$ this further means that we can rely on the DFT for a faster compuation.

Proposition 4. *For any matrices $\mathbf{L_f}, \mathbf{L_e}$, there exists a BCCB matrix $\mathbf{H}_{\max} \in \mathbf{H}^V$ such that*

$$\max_{\mathbf{H} \in \mathbf{H}^V} \|\mathbf{L_f} - \mathbf{L_e}\mathbf{H}\|_1 = \|\mathbf{L_f} - \mathbf{L_e}\mathbf{H}_{\max}\|_1.$$

Proof. Assume that the maximum is achieved with the matrix $\mathbf{H}'_{\max}$. Then,

$$\max_{\mathbf{H} \in \mathbf{H}^V} \|\mathbf{L_f} - \mathbf{L_e}\mathbf{H}\|_1 = \sum_{i=1}^{MN} \sum_{l=1}^{MN} |[\mathbf{L_f}]_{ij} - [\mathbf{L_e}]_{il}[\mathbf{H}'_{\max}]_{lj}|$$

for some $j = 1, 2, \ldots, MN$. Now recalling that each matrix in $\mathrm{Circ}(M, N)$ can be uniquely identified by a single column, we can extend the j-th column of $\mathbf{H}'_{\max}$ to a matrix that is in $\mathrm{Circ}(M, N)$. Such a matrix would also be in $\mathbf{H}^V$ since the entries $[\mathbf{H}'_{\max}]_{lj} \in \{[\underline{\mathbf{H}}]_{lj}, [\bar{\mathbf{H}}]_{lj}\}$ for all $l, j \in \mathbb{Z}_{MN}$. □

Appendix C
Proof of the Monotonic-Convergence Radius

The notions of asymptotic stability and monotonic convergence can also be studied over the error recursion equation, which amounts to analyzing the maximal spectral radius or maximal norm of $\mathbf{I} - \mathbf{H}\mathbf{L_e}$ over the set $\mathbf{H}^I$, when the special case of $\mathbf{L_f} = \mathbf{I}$ is considered. Note that asymptotic stability can equivalently be considered in either the input vector or the output vector, but monotonic convergence is specific to a single vector sequence, the input or the output.

The results of [20] are mostly specific to the perfect tracking case $\mathbf{L_f} = \mathbf{I}$ and proceed by considering the matrix $\mathbf{I} - \mathbf{H}\mathbf{L_e}$. However, it is straightforward to check that the validity of Theorems 5.3 and 5.6 of [20] by making the appropriate substitutions, as we have discussed in Section IV for the interval stability radius. For the other change as it relates to the monotonic-convergence radius, we do the following. Instead of the matrix ΔT_s defined on page 60 of [20], define the augmented perturbation matrix as

$$\Delta_{\mathbf{L_e}\mathbf{H}}^{\mathrm{aug}} \triangleq \begin{bmatrix} 0 & (\mathbf{L_e}\mathbf{H}_\delta)^* \\ \mathbf{L_e}\mathbf{H}_\delta & 0 \end{bmatrix},$$

where $\mathbf{H}_\delta$ is the plant perturbation. Then since $\Delta_{\mathbf{L_e}\mathbf{H}}^{\mathrm{aug}}$ is symmetric, its spectral radius and maximal singular value are equal. Thus, denoting by $\bar{\lambda}(.)$ the spectral radius, and by $\bar{\sigma}(.)$ the maximal singular value, we have

$$\begin{aligned} \left\| \Delta_{\mathbf{L_e}\mathbf{H}}^{\mathrm{aug}} \right\|_2 &= \bar{\sigma}(\Delta_{\mathbf{L_e}\mathbf{H}}^{\mathrm{aug}}) = \bar{\lambda}(\Delta_{\mathbf{L_e}\mathbf{H}}^{\mathrm{aug}}) \\ &= \bar{\sigma}(\mathbf{L_e}\mathbf{H}_\delta) = \|\mathbf{L_e}\mathbf{H}_\delta\|_2 \leq \|\mathbf{L_e}\|_2 \|\mathbf{H}_\delta\|_2, \end{aligned}$$

where the third equality can be verified from block matrix determinant formulas. Therefore, the inequality

$$\left\| \Delta_{\mathbf{L_e}\mathbf{H}}^{\mathrm{aug}} \right\|_2 \leq \|\mathbf{L_e}\|_2 \|\mathbf{H}_\delta\|_2$$

can be used in lieu of the inequality (5.33) on page 61 of [20], to arrive at (11).

Acknowledgment

The authors would like to acknowledge Christopher P. Pannier for his help editing this manuscript.

References

[1] Y. Huang, M. C. Leu, J. Mazumder, and A. Donmez, "Additive Manufacturing: Current State, Future Potential, Gaps and Needs, and Recommendations," *Journal of Manufacturing Science and Engineering*, vol. 137, no. 1, p. 014001, Feb. 2015. [Online]. Available: http://manufacturingscience.asmedigitalcollection.asme.org/article.aspx?doi=10.1115/1.4028725

[2] L. Robinson and J. Scott, "Layers of Complexity: Making the Promises Possible for Additive Manufacturing of Metals," *JOM*, vol. 66, no. 11, pp. 2194–2207, Nov. 2014. [Online]. Available: http://link.springer.com/10.1007/s11837-014-1166-x

[3] Y. Xie, L. E. Rustom, A. M. McDermott, J. D. Boerckel, A. J. Wagoner Johnson, A. G. Alleyne, and D. J. Hoelzle, "Net shape fabrication of calcium phosphate scaffolds with multiple material domains," *Biofabrication*, vol. 8, no. 1, p. 015005, 2016. [Online]. Available: http://stacks.iop.org/1758-5090/8/i=1/a=015005

[4] E. Sachs, E. Wylonis, S. Allen, M. Cima, and H. Guo, "Production of injection molding tooling with conformal cooling channels using the three dimensional printing process," *Polymer Engineering & Science*, vol. 40, no. 5, pp. 1232–1247, May 2000. [Online]. Available: http://doi.wiley.com/10.1002/pen.11251

[5] U. Thombansen, A. Gatej, and M. Pereira, "Process observation in fiber laserbased selective laser melting," *Optical Engineering*, vol. 54, no. 1, p. 011008, Oct. 2014. [Online]. Available: http://opticalengineering.spiedigitallibrary.org/article.aspx?doi=10.1117/1.OE.54.1.011008

[6] Y. Wang, F. Gao, and F. J. Doyle III, "Survey on iterative learning control, repetitive control, and run-to-run control," *Journal of Process Control*, vol. 19, no. 10, pp. 1589 – 1600, 2009. [Online]. Available: http://www.sciencedirect.com/science/article/pii/S0959152409001681

[7] P. M. Sammons, D. A. Bristow, and R. G. Landers, "Height Dependent Laser Metal Deposition Process Modeling," *Journal of Manufacturing Science and Engineering*, vol. 135, no. 5, p. 054501, Sep. 2013. [Online]. Available: http://manufacturingscience.asmedigitalcollection.asme.org/article.aspx?doi=10.1115/1.4025061

[8] D. Hoelzle, A. Alleyne, and A. Johnson, "Basis task approach to iterative learning control with applications to micro-robotic deposition," *Control Systems Technology, IEEE Transactions on*, vol. 19, no. 5, pp. 1138–1148, Sept 2011.

[9] S. Lupashin, A. Schllig, M. Sherback, and R. D'Andrea, "A simple learning strategy for high-speed quadrocopter multi-flips," in *2010 IEEE International Conference on Robotics and Automation*, May 2010, pp. 1642–1648.

[10] H.-S. Ahn, Y.-Q. Chen, and K. Moore, "Iterative learning control: Brief survey and categorization," *Systems, Man, and Cybernetics, Part C: Applications and Reviews, IEEE Transactions on*, vol. 37, no. 6, pp. 1099–1121, 2007.

[11] D. Bristow, M. Tharayil, and A. Alleyne, "A survey of iterative learning control," *Control Systems, IEEE*, vol. 26, no. 3, pp. 96–114, 2006.

[12] D. J. Hoelzle and K. L. Barton, "On spatial iterative learning control via two dimensional convolution: Stability analysis and computational efficiency," *IEEE Trans. on Control Systems Technology*, no. 4, pp. 1504–1512, 2016.

[13] K. L. Moore and Y. Chen, "Iterative learning control approach to a diffusion control problem in an irrigation application," in *2006 International Conference on Mechatronics and Automation*, June 2006, pp. 1329–1334.

[14] C. T. Freeman, P. L. Lewin, E. Rogers, D. H. Owens, and J. J. Hatonen, "Discrete Fourier transform based iterative learning control design for linear plants with experimental verification," *ASME Journal of Dynamic Systems, Measurement, and Control*, vol. 131, no. 3, pp. 031 006–031 006–10, Jul 2009.

[15] E. Rogers, K. Galkowski, and D. H. Owens, *Control Systems Theory and Applications for Linear Repetitive Processes*. Berlin: Springer-Verlag, 2007.

[16] W. Hakvoort, R. Aarts, J. van Dijk, and J. Jonker, "A computationally efficient algorithm of iterative learning control for discrete-time linear time-varying systems," *Automatica*, vol. 45, no. 12, pp. 2925 – 2929, 2009. [Online]. Available: http://www.sciencedirect.com/science/article/pii/S0005109809004336

[17] H. Sun and A. G. Alleyne, "A computationally efficient norm optimal iterative learning control approach for LTV systems," *Automatica*, vol. 50, no. 1, pp. 141 – 148, 2014. [Online]. Available: http://www.sciencedirect.com/science/article/pii/S0005109813004421

[18] K. L. Barton, D. A. Bristow, and A. G. Alleyne, "A numerical method for determining monotonicity and convergence rate in iterative learning control," *International Journal of Control*, vol. 83, no. 2, pp. 219–226, 2010. [Online]. Available: http://dx.doi.org/10.1080/00207170903131177

[19] G. Golub and C. F. V. Loan, *Matrix Computations*. Baltimore, MD: The Johns Hopkins University Press, 1996.

[20] H.-S. Ahn, K. L. Moore, and Y. Chen, *Iterative Learning Control: Robustness and Monotonic Convergence for Interval Systems*. London: Springer, 2007.

[21] ——, "Stability analysis of discrete-time iterative learning control systems with interval uncertainty," *Automatica*, vol. 43, no. 5, pp. 892 – 902, 2007. [Online]. Available: http://www.sciencedirect.com/science/article/pii/S0005109807000258

[22] V. D. Blondel, J. Theys, , and J. N. Tsitsiklis, "When is a pair of matrices stable?" in *Unsolved Problems in Mathematical Systems and Control Theory*, V. D. Blondel and A. Megretski, Eds. Princeton, NJ: Princeton University Press, 2004, pp. 304–308.

[23] H.-S. Ahn and Y. Q. Chen, "Exact maximum singular value calculation of an interval matrix," *Automatic Control, IEEE Transactions on*, vol. 52, no. 3, pp. 510–514, March 2007.

[24] B. Chu and D. H. Owens, "Iterative learning control for constrained linear systems," *International Journal of Control*, vol. 83, no. 7, pp. 1397–1413, 2010. [Online]. Available: http://dx.doi.org/10.1080/00207171003758752

[25] S. Mishra, U. Topcu, and M. Tomizuka, "Optimization-based constrained iterative learning control," *Control Systems Technology, IEEE Transactions on*, vol. 19, no. 6, pp. 1613–1621, Nov 2011.

[26] ——, "Iterative learning control with saturation constraints," in *American Control Conference, 2009. ACC '09.*, June 2009, pp. 943–948.

[27] J. H. Lee, K. S. Lee, and W. C. Kim, "Model-based iterative learning control with a quadratic criterion for time-varying linear systems," *Automatica*, vol. 36, no. 5, pp. 641 – 657, 2000. [Online]. Available: http://www.sciencedirect.com/science/article/pii/S0005109899001946

[28] S. Gunnarsson and M. Norrlöf, "On the design of ILC algorithms using optimization," *Automatica*, vol. 37, no. 12, pp. 2011 – 2016, 2001. [Online]. Available: http://www.sciencedirect.com/science/article/pii/S0005109801001546

[29] C.-T. Chen and S.-T. Peng, "Learning control of process systems with hard input constraints," *Journal of Process Control*, vol. 9, no. 2, pp. 151 – 160, 1999. [Online]. Available: http://www.sciencedirect.com/science/article/pii/S0959152498000389

[30] P. M. Sammons, M. L. Gegel, D. A. Bristow, and R. G. Landers, "Repetitive process control of additive manufacturing with application to laser metal deposition," *IEEE Transactions on Control Systems Technology*, pp. 1–10, 2018.

[31] B. Altın and K. Barton, "Exponential stability of nonlinear differential repetitive processes with applications to iterative learning control," *Automatica*, vol. 81, pp. 369 – 376, 2017. [Online]. Available: http://www.sciencedirect.com/science/article/pii/S0005109817301772

[32] B. Altin and K. Barton, "Robust iterative learning for high precision motion control through $\mathcal{L}_1$ adaptive feedback," *Mechatronics*, vol. 24, no. 6, pp. 549 – 561, 2014, control of High-Precision Motion Systems. [Online]. Available: http://www.sciencedirect.com/science/article/pii/S0957415814000713

[33] B. Altın, J. Willems, T. Oomen, and K. Barton, "Iterative learning control of iteration-varying systems via robust update laws with experimental implementation," *Control Engineering Practice*, vol. 62, pp. 36 – 45, 2017. [Online]. Available: http://www.sciencedirect.com/science/article/pii/S0967066117300345

[34] S. Saab, "Optimality of first-order ILC among higher order ILC," *Automatic Control, IEEE Transactions on*, vol. 51, no. 8, pp. 1332–1336, Aug 2006.

[35] S. Devasia, "Should model-based inverse inputs be used as feedforward under plant uncertainty?" *Automatic Control, IEEE Transactions on*, vol. 47, no. 11, pp. 1865–1871, Nov 2002.

[36] C. Pannier, L. Ojeda, Z. Wang, D. J. Hoelzle, and K. Barton, "An electrohydrodynamic jet printer with integrated metrology," *Mechatronics*, p. to appear, 2018.

[37] J. Park, M. Hardy, S. J. Kang, K. Barton, K. Adair, D. Mukhopadhyay, C. Y. Lee, M. S. Strano, A. G. Alleyne, J. G. Georgiadis, P. M. Ferreira, and J. A. Rogers, "High-resolution electrohydrodynamic jet printing," *Nature Materials*, vol. 6, pp. 782–789, 2007.

[38] Z. Wang, P. Sammons, C. Pannier, K. Barton, and D. J. Hoelzle, "System identification of a discrete repetitive process model for electrohydrodynamic jet printing," in *Proceedings of the IEEE American Control Conference*, Milwaukee, WI, 2018.

[39] Z. Wang, C. P. Pannier, K. Barton, and D. J. Hoelzle, "Application of robust monotonically convergent spatial iterative learning control to microscale additive manufacturing," *Accepted to IFAC Mechatronics*, 2018.

Berk Altın received his B.S. in Mechatronics from Sabancı University in 2011, Istanbul, Turkey in 2011. From 2011 to 2016, he attended the University of Michigan, Ann Arbor, as a Fulbright fellow, where he received the M.S. and Ph.D. degrees in Electrical Engineering: Systems, and the M.S. degree in Mathematics, in 2013, 2016 and 2016, respectively. He is currently employed as a postdoctoral researcher at the University of California, Santa Cruz, with the Hybrid Systems Laboratory. His primary research interests include hybrid systems, model predictive control, iterative learning control, repetitive processes, and multidimensional systems, with applications in cyber-physical systems, power systems, robotics, and additive manufacturing.

Zhi Wang Dr. Zhi Wang received his Ph.D. in Mechanical Engineering from the University of Notre Dame in 2018 under the advisement of Prof. David Hoelzle and Prof. Panos Antsaklis, and his B.Eng. in Mechanical Engineering from Tsinghua University in 2013. The research interests of Dr. Wang include learning control algorithms and their application to additive manufacturing technologies.

David J. Hoelzle is an Assistant Professor in the Department of Mechanical and Aerospace Engineering at the Ohio State University. He received his MS and PhD from the University of Illinois at Urbana-Champaign in 2007 and 2011, respectively, in Mechanical Science and Engineering and his BS from the Ohio State University in 2005 in Mechanical Engineering. Between his PhD and current position, he completed a post-doc in the Department of Integrative Biology and Physiology at the University of California, Los Angeles and held the position of Assistant Professor in the Department of Aerospace and Mechanical Engineering at the University of Notre Dame. His research interests lie in applied control theory and dynamics for applications in additive manufacturing robotics and microsystems for mechanobiology research. Prof. Hoelzle is a recipient of the 2016 CAREER Award and the 2016 Society of Manufacturing Engineers Outstanding Young Manufacturing Engineer Award.

Kira Barton Kira Barton is an Associate Professor and Miller Faculty Scholar in the Department of Mechanical Engineering at the University of Michigan. She received her B.Sc. in Mechanical Engineering from the University of Colorado at Boulder in 2001. She continued her education in mechanical engineering at the University of Illinois at Urbana-Champaign and completed her M.Sc. and Ph.D. degrees in 2006 and 2010, respectively. She held a postdoctoral research position at the University of Illinois from Fall 2010 until Fall 2011, at which point she joined the Mechanical Engineering Department at the University of Michigan at Ann Arbor. Kira conducts research in modeling, sensing, and control for applications in advanced manufacturing and robotics, with a specialization in iterative learning control and micro-additive manufacturing. Kira is the recipient of an NSF CAREER Award in 2014, 2015 SME Outstanding Young Manufacturing Engineer Award, the 2015 University of Illinois, Department of Mechanical Science and Engineering Outstanding Young Alumni Award, the 2016 University of Michigan, Department of Mechanical Engineering Department Achievement Award, and the 2017 ASME Dynamic Systems and Control Young Investigator Award.